Astron. Astrophys. 326, 565–579 (1997)

ASTRONOMY
AND
ASTROPHYSICS

A surprising correlation between X-ray and Hα morphologies in early-type galaxies

G. Trinchieri[1,2], **L. Noris**[3], **and S. di Serego Alighieri**[4]

[1] Osservatorio Astronomico di Brera, Via Brera 28, I-20121 Milano Italy
[2] Max Planck Institut für extraterrestrische Physik, Giessenbachstraße, D-85740 Garching, Germany
[3] Università degli Studi di Milano, Via Celoria 16, I-20133 Milano, Italy
[4] Osservatorio Astrofisico di Arcetri, Largo E. Fermi 5, I-50125 Firenze, Italy

Received 27 February 1997 / Accepted 23 May 1997

Abstract. High resolution X-ray images of three early type galaxies observed with the ROSAT HRI are presented. Data for NGC 1553 and NGC 5846 indicate that the emission is highly irregular, with interesting features on scales from a few arcsec to a few arcmin. The gas temperatures also vary both with the galactocentric radius and in correspondence to regions of higher emission and denser material.

Strikingly similar features are observed in the X-ray and Hα morphologies of NGC 1553 and NGC 5846, while smoother, more regular isophotes are observed in NGC 4649 at both wavelengths. A connection between these two kinds of emission therefore seems likely. In the light of our observations we discuss possible scenarios that can account for the connection between X-ray and Hα emissions.

Key words: X-rays: galaxies – galaxies: elliptical and lenticular – galaxies: ISM – galaxies: individual: NGC 1553; NGC 4649; NGC 5846

1. Introduction

The existence of a hot interstellar medium in bright early-type galaxies and some of its properties have been established in the past $\sim$ 15 years with data first from *Einstein* and more recently from ROSAT and ASCA. X-ray images have shown the presence of diffuse emission at least coextensive with the stellar component in the X-ray bright early type galaxies. Average temperatures and radial temperature gradients have been measured. In general, gas temperatures of 0.5–1.5 keV are common, and cooling times are typically much shorter than a Hubble time.

Coexisting with the hot interstellar medium (ISM), a cooler ("warm") component has been mapped in Hα in several X-ray bright objects (Kim 1989; Trinchieri & di Serego 1991; Shields 1991; Goudfrooij et al. 1994; Buson et al. 1994; Singh et al. 1995; di Serego et al. in preparation). The morphology of this emission can either be relatively smooth and azimuthally symmetric or exhibit filamentary structures, arcs and/or rings. Although clearly extended, it is generally confined to the innermost regions of the galaxies, and it is relatively faint and hard to detect properly. To date, the study of the relation between hotter and cooler gas has been restricted to a handful of galaxies, and mostly to the statistical comparison of the total X-ray and Hα luminosities. Detailed studies of the morphology of the gas require high-resolution X-ray data which are only now becoming available with the ROSAT HRI observations. The comparison of the luminosities in optical emission lines and in X-rays suggests that while galaxies with a larger X-ray emitting gas component also show more powerful line emission than objects with a poorer hot ISM, the scatter in the relation is significant, implying that other parameters play a role in the production of optical lines (see *e.g.*, Trinchieri & di Serego 1991).

There are however new high resolution data at both X-ray and optical wavelengths that suggest a very close connection between these two gas phases. As shown by the preliminary data presented by Trinchieri & Noris (1995), both gross and finer morphological similarities are found in the X-ray and Hα maps of NGC 1553 and NGC 5846. We present here a more comprehensive investigation of these similarities. Sects. 2 and 3 present the X-ray data analysis of NGC 1553, NGC 4649 and NGC 5846. The Hα data obtained from the literature (Trinchieri & di Serego 1991, di Serego et al. in preparation) are compared to the X-ray maps in Sect. 4, and a discussion of the results is presented in Sect. 5.

2. Data analysis: HRI observations

ROSAT HRI data of the sample galaxies have been obtained in several observing runs, as detailed in Table 1. Standard analysis procedures have been applied to the data, as briefly summarized below. To analyze the X-ray data we have used mainly the PROS software (Worrall et al. 1992) developed under the IRAF (Tody 1986) environment. For each field, a radial distribution

Send offprint requests to: G. Trinchieri

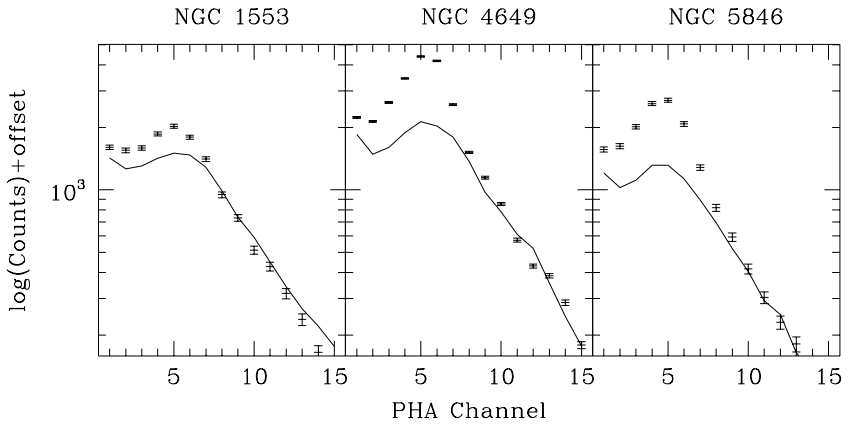

Fig. 1. PHA distribution of the photons in the "source" and in the "background" regions. The "source" region (crosses with errorbar) is a circle of radius r=5′, 5′, and 7′ for NGC 1553, NGC 4649 and NGC 5846 respectively. The "background" (solid line) is extracted from an annulus at $8' - 10'$.

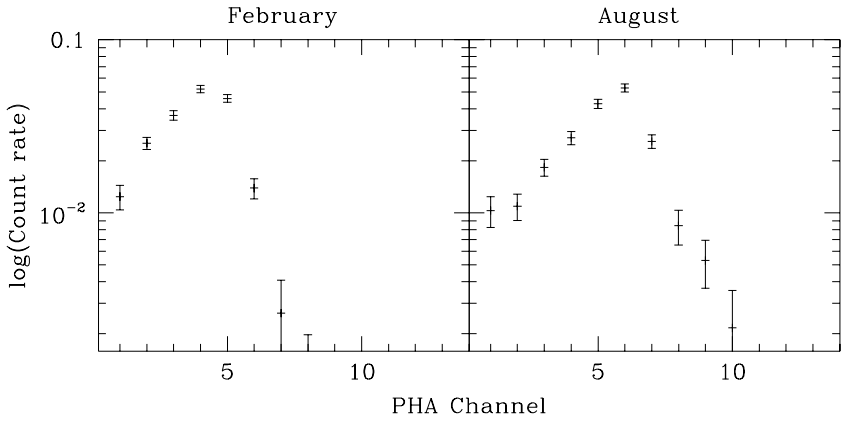

Fig. 2. PHA distribution of the net count rate extracted from a circle of 5′ radius in the February (left) and August (right) observations of NGC 5846

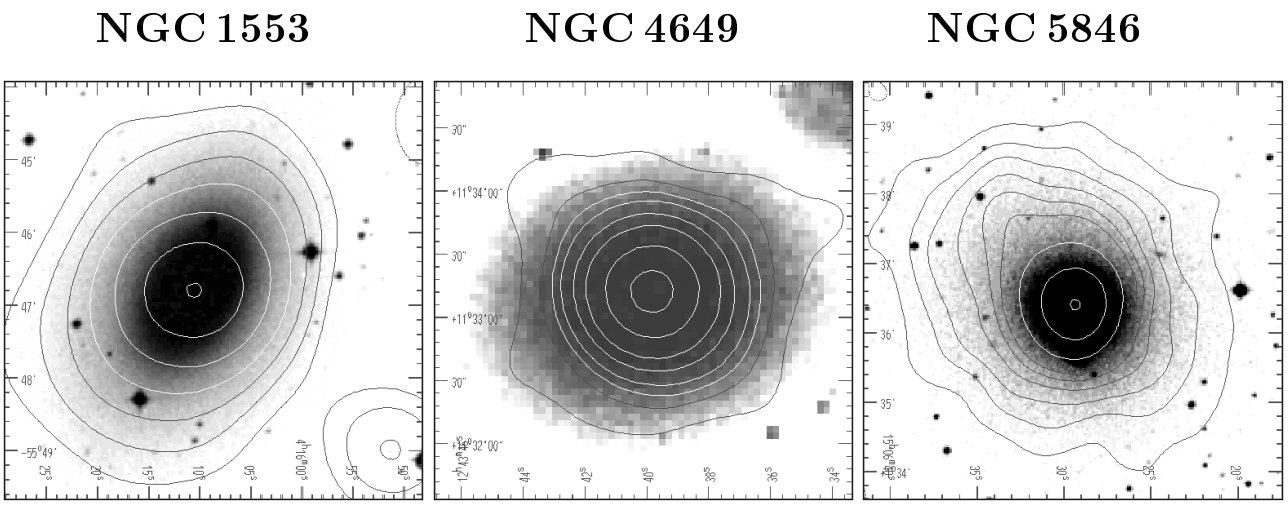

Fig. 3. X-ray isointensity contours superposed onto the optical images from the Digitized Sky Survey. Note that the scale is different in the three figures and reflects the X-ray data shown in Figs. 4d, 5b and 6d respectively.

of the detected emission is produced in concentric annuli centered at the X-ray peak and extending out to the edges of the field. The radial profiles indicate that outside of r=5′, 5′ and 7′ for NGC 1553, NGC 4649 and NGC 5846 respectively, the emission is relatively constant with radius, as expected from an uniform illumination (such as due to isotropic sky emission and particle contamination) of the instrument field of view (ROSAT HRI Calibration Report). We have therefore used the region outside of these radii to estimate the background. Even though a small vignetting effect is evident in the form of a radial gradient in the data, the correction is small, and a local estimate allows us to better take into account the statistical uncertainties in the subtraction of the background (however, this is relevant only at the outskirts of the emission). To minimize the vignetting effect

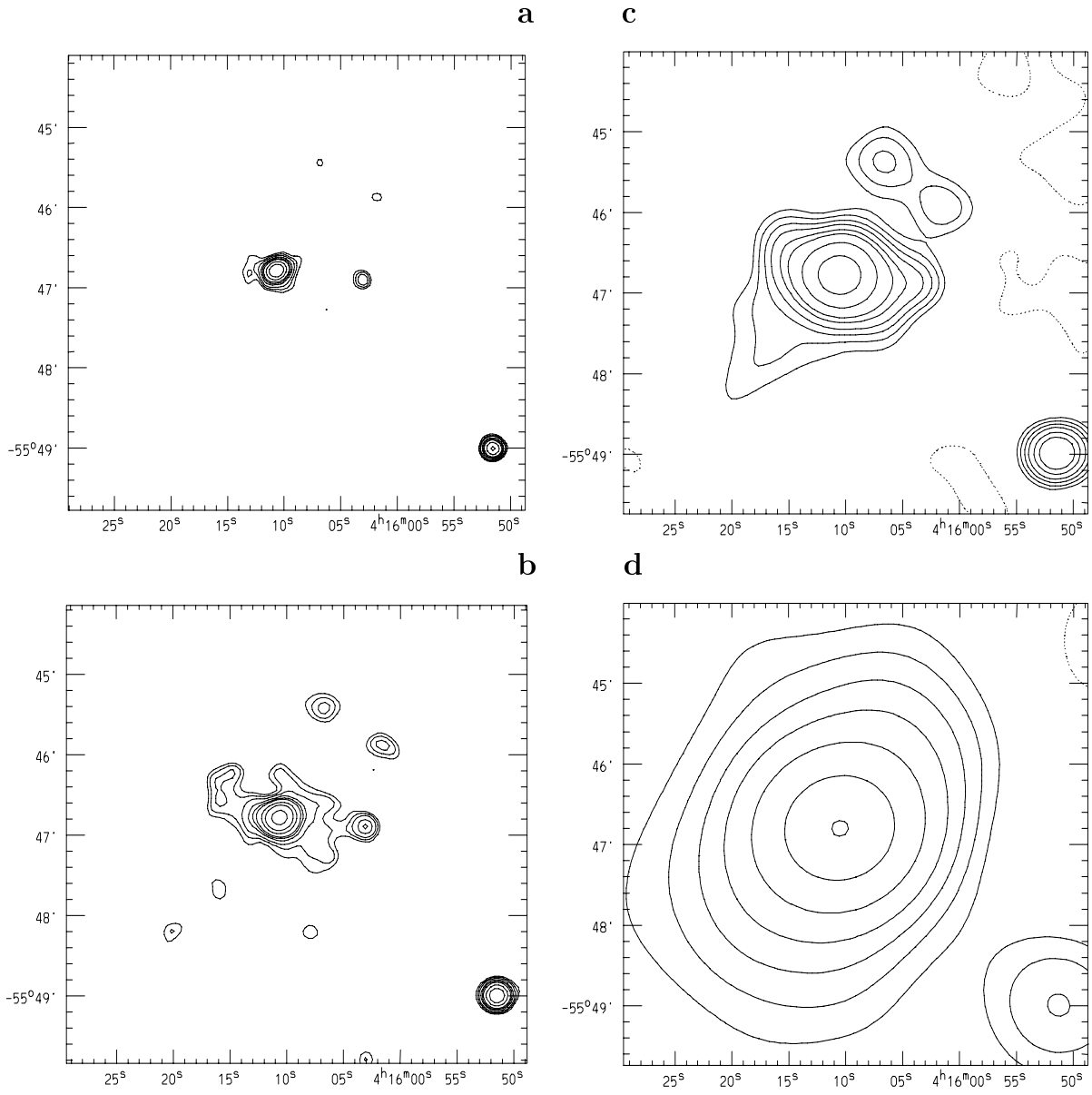

Fig. 4a–d. Iso-intensity contour maps of NGC 1553. Images of different pixel size have been smoothed with Gaussian smoothings of different σ as indicated later. A locally determined background is subtracted (see text). The dashed contour indicates 0 counts/pixel. **a**: $\sigma = 4''$, from an image with a pixel size of $2''$. Contour levels are 0.45, 0.63, 0.9, 1.5, 2.8 counts/pixel; **b**: $\sigma = 6''$, from an image with a pixel size of $3''$. Contour levels are 0.39 0.5 0.63 0.86 1.05 1.25 1.8 2.5 4 counts/pixel; **c** and **d**: $\sigma = 16''$ and $\sigma = 40''$ respectively, from an image with a pixel size of $4''$. Contours at 0.33 0.41 0.50 0.6 0.75 0.9 1.3 2 2.8 counts/pixel and 0.13 0.18 0.24 0.32 0.45 0.65 0.85 counts/pixel respectively.

we have selected the annulus at $8' - 10'$ radial distances for all objects, that should avoid emission from the source, while being relatively near the field's center.

The HRI has not been calibrated in energy, however the data retain the information about the Pulse Height Amplitude Channel (PHA, in the range 1 to 15, see The ROSAT Users' Handbook) in which each incoming photon was detected. Therefore, although we cannot retrieve the energy distribution of the photons, we can examine the PHA of the photons extracted from different regions to look for differences. On the other hand, the distribution in PHA channels is strongly dependent on the gain of the detector ($i.e.$ the position of the peak of the PHA distribution obtained from the observation of the lines [C, Cu, and Al] used for calibration purposes), which is not constant over the detector and it is not constant in time (see The ROSAT Users' Handbook). Therefore a detailed comparison between different PHA distributions must take into account both spatial and temporal variations of the gain, which can mimic significant differences that are not real. However, when large areas and a large enough PHA range are considered, these variations tend to average out, and therefore a selection in PHA channels could still be useful for example to enhance the significance of the

Table 1. Log of the HRI and PSPC observations of the galaxies discussed

Name	R.A. Dec. (J2000)	begin/end	Obs. Time (sec)	H/P
NGC1553	04 16 10.4	14/06/94-26/08/94	46149	H
	−55 46 51	19/08/93-24/09/93	15320	P
NGC4649	12 43 40.3	11/07/94-11/07/94	2196	H
	+11 32 58	17/06/95-18/06/95	11827	H
		21/12/91-27/12/91	14301	P
NGC5846	15 06 29.4	02/02/94-05/02/94	22581	H
	+01 36 25	05/08/94-11/08/94	16763	H
		25/07/92-05/08/93	8808	P
		18/01/93-18/01/93	5947	P

NOTE: H/P indicates which ROSAT instrument (HRI or PSPC) was used

detection. In fact the spectral distribution of the "source" and of the background are different, as shown in Fig 1. We have therefore used only those PHA channels in which the signal is significantly higher than the background, namely PHA 1 to 7 for NGC 1553, PHA 1 to 10 for NGC 4649, and PHA 1 to 9 for NGC 5846.

Both NGC 4649 and NGC 5846 were observed on two occasions by the ROSAT HRI, as reported in Table 1. In both cases we have merged the data and used the result for our analysis, after checking the single observations for consistency. The first observation of NGC 4649 is of only $\sim$ 2000 sec., while the second observation is much longer ($\sim$ 12000 sec.), and will therefore dominate in the subsequent analysis. The two observations of NGC 5846 are of similar length, and therefore each will have approximately equal weight in the final merged image. We have therefore first analyzed each of the two images separately, to check for possible differences. With the exception of the distribution of the emission in PHA channels (cf. Fig. 2), we have found that the two sets of observations are consistent. A gain variation with time is expected to be responsible for the difference in the PHA distribution, as reported in the HRI calibration report (The ROSAT Users' Handbook) and therefore should not be indicative of an intrinsic change of the source characteristics. Since the details of the PHA distribution have not been exploited (also in consideration of the gain variations, as briefly discussed above), rather the integrated PHA range has been considered, we have disregarded this difference and used the merged image for the analysis.

2.1. X-ray maps

Background subtracted X-ray images were then calculated for all galaxies. To enhance different details, the raw data have been binned and smoothed with Gaussian functions of increasing σ's. Fig 3 shows the lowest spatial resolution X-ray contours superposed onto the optical images from the "Digitized Sky Survey"[1]. The results are described briefly below for each galaxy.

NGC 1553 The iso-intensity contour maps of Fig. 4a–d show that the emission from NGC 1553 is complex and clearly deviates from azimuthal symmetry. The low resolution map is elongated similarly to the optical light (optical PA=146°, Kormendy 1984; see Fig. 4a–dd). At higher resolution, several features can be clearly identified: an extension towards the SE (almost like a "tail") is visible towards the SE (c); the central region appears elongated along the $\sim$ E-W direction, roughly perpendicular to the outer elongation and the optical PA (b,c). This is however further resolved in a possible spiral-like structure (b) around the central peak (a), plus a more isolated source to the W (given the limited statistics the source could be consistent with a point-source). Two additional features can also be seen to the NW, at a distance of $\geq 1.'5$ from the center (b,c).

NGC 4649 As evident from the maps in Fig. 5a and b, the X-ray emission from NGC 4649 is regular and roughly azimuthally symmetric, as already shown by the PSPC data (Trinchieri et al. 1997). In the innermost regions the X-ray isophotes appear somewhat compressed in the SW quadrant but the emission is smooth and no small scale features appear at higher resolution.

NGC 5846 The maps at different resolutions (Fig. 6a–d) all indicate that the emission from this galaxy is highly asymmetric and clumpy. The elongation in the NE-SW direction that is visible in the low resolution image (Fig. 6d) is clearly resolved in a feature extending in the NE quadrant, and most prominent at $1' - 2'$ radial distance from the peak (see Sect. 2.2 later and Fig. 7). At smaller radii the emission is also skewed, with a steeper gradient on the Western side (see Sect. 2.3) and an elongation to the South. Several features that can be described as clumps, holes and filaments (Fig. 6a) can also be observed at radii smaller than $\sim 0.'5 - 1'$.

2.2. Azimuthal profiles

The qualitative statements that the emission from NGC 1553 and NGC 5846 is not azimuthally symmetric have been checked more quantitatively by analyzing the azimuthal distribution of the emission. For all galaxies, we have divided the emission from the galaxy, namely a circle of radius $5'$ for NGC 1553 and NGC 4649, and $7'$ for NGC 5846, in 8-10 azimuthal sectors. The results are plotted in Fig. 7. The azimuthal dependence of the emission is almost nonexistent for NGC 4649, while strong deviations from a constant are observed for the other two objects.

We have further analyzed the azimuthal distribution of the emission of each object in separate concentric annuli, as described below for each of them. All angles are measured counterclockwise from North.

[1] Based on photographic data of the National Geographic Society – Palomar Observatory Sky Survey (NGS-POSS) obtained using the Oschin Telescope on the Palomar Mountain. The NGS-POSS was funded by a grant from the National Geographic Society to the California Institute of Technology. The plates were processed into the present compressed digital form with their permission. The Digitized Sky Survey was produced at the Space Telescope Science Institute under US Government grant NAG W-2166.

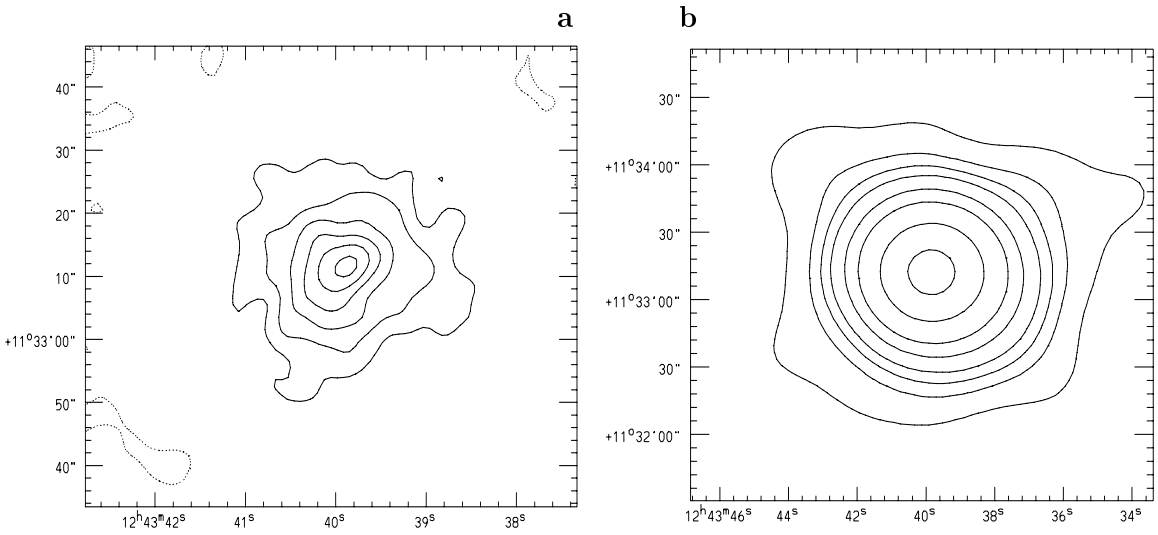

Fig. 5a and b. As in Fig. 4a–d for NGC 4649. The scale in **a** is $\sim 1/3$ that in **b**. **a**: σ = 2″, from an image with a pixel size of 2″. Contours at 0.3 0.6 0.9 1.4 1.8 2.2 counts/pixel; **b**: σ = 15″, from an image with a pixel size of 3″. Contours at 0.2 0.3 0.4 0.6 0.9 1.3 2.3 3.7 counts/pixel.

NGC 1553 The 5′ region of the emission has been divided into 3 annuli of $0' - 1'$; $1' - 3'$; $3' - 5'$ inner and outer radii respectively, and 6 to 8 azimuthal sectors. Deviations from azimuthal symmetry are present in all three annuli, although more evident in the $1' - 3'$ region. The "point source" to the W of the central region is visible in the $0' - 1'$ annulus at an angle of $\sim 250°$, while the $\sim$ N-S elongation is visible in the $1' - 3'$ region (see Fig. 4). A peak at $\sim 210°$ visible in the $3' - 5'$ annulus corresponds to the probably unrelated source visible in the SW quadrant. The "dip" at angles $\sim 0° - 45°$ in the innermost region corresponds to the hole in the emission between the central source and the "spiral-type" structure visible in the X-ray contours of Fig. 4c.

NGC 4649 As shown by Fig. 7, no significant deviations from azimuthal symmetry are observed in this galaxy on all scales. Marginal differences are evident if the $\sim$ 0°–45° azimuthal region is compared to the $\sim$ 270°–300° region, in the 0′–5′ annulus, which is probably due to the regions outside the central 1′ (Fig. 7, bottom).

NGC 5846 The azimuthal distribution is divided in three annuli ($0' - 1'$, $1' - 2.'5$, and $2.'5 - 5'$) and in 10 azimuthal sectors. While the innermost $\sim 1'$ circle is relatively flat, and shows only the skewness of the emission to the W, the feature to the N is prominent in the $\sim 1' - 2.'5$ annulus (from $\sim 340°$ to $\sim 90°$). The $\sim$ ellipsoidal shape of the emission at larger radii is visible in the outermost annulus.

2.3. Radial profiles

The surface brightness distribution of the emission from each galaxy, obtained in concentric annuli, is shown in Fig. 8. As expected from the morphology of the emission discussed above, the radial profiles of all but NGC 4649 are not smooth functions of radius. We have attempted to parameterize the radial profiles with a two parameter model ("King-type" model of the form $\Sigma_x \propto (1 + (\frac{r}{r_x})^2)^{(-3\beta+0.5)}$, with r_x as the core radius and β that indicates the radial dependence). To take into account the Point Spread Function (PSF) of the HRI, we have convolved the "King-type" model with the HRI PSF, as given in the "ROSAT HRI Calibration Report". However, we have obtained a reasonable fit only for NGC 4649, for which $r_x \sim 4''$ and $\beta \sim$0.47.

For NGC 1553, a fit can be found outside 10″, for a $r_x \sim 25''$ and $\beta \sim 0.41$. Inside a radius of r=10″, there is a clear excess, consistent with the presence of an unresolved source.

For NGC 5846 a possible fit with $r_x \sim 15''$ and $\beta \sim 0.5$ shows a clear excess in the $0.'7 - 2.'5$ region. To take into account the azimuthal asymmetry of the emission of NGC 5846, radial profiles in different azimuthal intervals and along different directions have also been obtained. Fig. 9 shows the comparison between the profiles obtained in the azimuthal limits from 85° to 340° and from 340° and 85°, where the feature is visible. A significant excess in the $\sim 1' - 2.5'$ region is clearly seen. In fact, the model with r_x = 15″ and β = 0.5 reported on the data shows good agreement with the profile in the 85° to 340° region while making the excess in the NE quadrant prominent.

3. Spectral data from PSPC observations

All three galaxies have also been observed with the ROSAT PSPC, as indicated in Table 1. A detailed analysis of the PSPC data of these objects is beyond the scope of this work. However, the spectral information that is contained in the PSPC data is useful to derive fluxes and luminosities and to better study the characteristics of the ISM in these galaxies. We have therefore analyzed the PSPC data of NGC 1553 and NGC 5846 in the ROSAT archive. NGC 4649 results have been taken from Trinchieri et al. (1997). The analysis is done using the IRAF-PROS software, to be consistent with the results on NGC 4649

Table 2. Spectral characteristics of the emission in NGC 1553

Region	net counts and error	N_H $\log_{10}$	kT_1 (keV)	90% conf. limits	kT_2 (keV)	90% conf. limits	Normal. ratios[1]	χ^2_{min}	DOF	Notes
$0' - 2'$	980±38.6	18.00	3	> 2				47.5	22	A,B,C
		20.38	3					182.3	23	C,D
		20.38	0.133	0.115-0.155	1.057	0.90-1.45	-0.044	34.8	20	D
		18.00	0.308		3.0		0.732	13.9	20	A,B
$0' - 7'$	1587.6± 76.9	18.00	3	> 2				61.2	22	A,B,C
		20.38	3					149	23	C,D
		20.38	0.139	0.11-0.16	1.008	0.70-1.20	-0.195	31.2	21	D
		18.00	0.276		2.48		0.505	15.4	20	A

Notes:

1 Ratio between the normalization parameter of the second component relative to the first (log ($norm_2$/$norm_1$)).
A The program finds the lowest value in the allowed range of N_H values.
B The 90% upper limit to the galactic absorption, for 2 interesting parameters, is ~ 19.5
C The program finds the uppermost value in the allowed kT range.
D The N_H parameter has been fixed at the galactic value

Table 3. Spectral characteristics of emission in NGC 5846

Region	net counts and error	N_H	90% confidence limits	kT	90% confidence limits	χ^2_{min}	DOF	Notes
$0' - 1'$	2604.1±56	20.40	20.25-20.55	0.604	0.54-0.65	30.9	20	A
	2110.3±57	20.45	20.30-20.60	0.561	0.50-0.62	22.8	20	B
$1' - 2.'5$	2611.9±58.4	20.37	20.25-20.50	0.810	0.77-0.84	30.0	21	C
	2158.9±62.4	20.35	20.20-20.50	0.780	0.72-0.83	25.0	21	B
$2.'5 - 5'$	1161.6±53	20.52	20.20-21.00	0.959	0.90-1.06	26.2	21	
	848.6±55.0	20.50	20.10-21.5	0.996	0.86-1.12	19.1	21	B
$5' - 12'$	1857.0±132.3	20.01	–	0.803	0.60-0.96	46.15	21	D
$0' - 5'$	6396.62±94.3	20.36	20.25-20.50	0.752	0.73-0.79	78.2	22	E
	5982.7±96.6	20.34	20.25-20.45	0.747	0.72-0.78	61.7	22	B,F
.....								
$1' - 2.'5$								G
$85° - 340°$	±	20.34	20.10-20.60	0.818	0.76-0.88	8.7		
$340° - 85°$	±	20.105	<20.40	0.710	0.62-0.78	17.7		
$340° - 85°$	±	20.13	< 21	0.577	0.36-0.76	10.5		H

NOTES: The background is obtained from the $25'$–$27'$ annulus, unless otherwise noted.

A The χ^2_{min} is reduced to 16.8 if a two temperature model is adopted. The best fit parameters are: N_H=20.51; kT_1=0.554; kT_2=3 (Upper limit of the allowed range)
B The background is obtained from the adjacent annulus (of $1' - 2'$; $2.'5 - 4'$; and $5' - 9'$ inner and outer radii).
C The χ^2_{min} is reduced to 18.9 if a two temperature model is adopted. The best fit parameters are: N_H=20.45; kT_1=0.745; kT_2=3 (Upper limit of the allowed range)
D The χ^2_{min} is reduced to 25.5 if a two temperature model is adopted. The best fit parameters are: N_H=20.48; kT_1=0.674; kT_2=3 (Upper limit of the allowed range)
E The χ^2_{min} is reduced to 25.4 if a two temperature model is adopted. The best fit parameters are: N_H=20.46; kT_1=0.675; kT_2=2.9
F The χ^2_{min} is reduced to 24.7 if a two temperature model is adopted. The best fit parameters are: N_H=20.49; kT_1=0.365; kT_2=1.7
G The $1' - 2.'5$ annulus is divided into the two angular regions. The background is obtained from the $2.'5 - 4'$ annulus.
H The background is obtained in the $1'$–$2.'5$ region, with the exclusion of the $340°$–$85°$ sector.

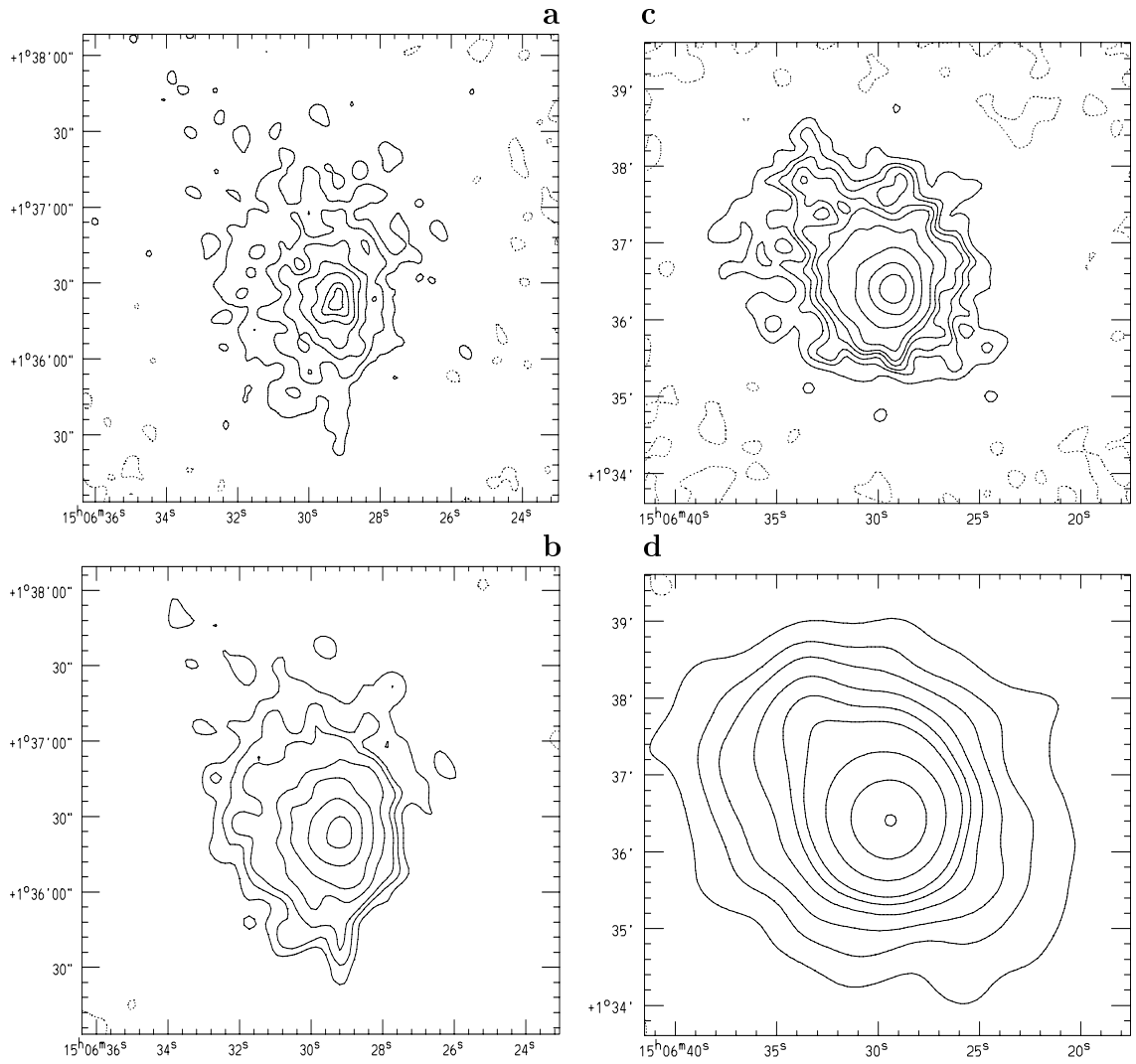

Fig. 6a–d. As in Fig. 4a–d for NGC 5846. The scale in **a,b** is $\sim 1/2$ that in **c,d**. **a**: $\sigma = 2\farcs5$, from an image with a pixel size of $2''$. Contours at 0.2, 0.34, 0.5, 0.75, 1, 1.35, 1.55 counts/pixel; **b**: $\sigma = 4''$, from an image with a pixel size of $2''$. Contours at 0.65, 0.85, 1.04, 1.5, 2.1, 3.3, 5; **c**: $\sigma = 6''$, from an image with a pixel size of $3''$. Contours at 0.6, 0.85, 1, 1.2, 1.4, 1.8, 3, 5, 8 counts/pixel; **d**: $\sigma = 9''$, from an image with a pixel size of $3''$. Contours at 0.2, 0.35, 0.5, 0.7, 0.9, 1.1, 1.7, 3 5 counts/pixel.

and with similar work on the spectral properties of early type galaxies (Trinchieri et al. 1994; 1997).

In order to estimate the total extent of the emission in the PSPC we have produced a radial distribution of the 0.2–2 keV photons binned in concentric annuli about the peak of the X-ray source, and compared it with the radial distribution of the data contained in the exposure map, that simulates the spatial response of the instrument to a constant incident source with a characteristics temperature of $\sim$1 keV. The unrelated sources that are also detected in the fields have been masked out in this comparison. Since the two radial distributions appear very similar at radii of $7'$ and $> 12'$ for NGC 1553 and NGC 5846 respectively, the region of the field outside these radii can be used to estimate the background (see also Trinchieri et al. 1994, 1997). To minimize the effect of vignetting, an annulus as close as possible to the source is used to estimate the background. For NGC 1553 the $7' - 10'$ annulus appears free of sources and can be used for this purpose. For NGC 5846 however, in order to avoid the circular support structure of the PSPC, the annulus at $25' - 27'$ has been used.

To estimate the gas temperature, we have assumed a thermal plasma model (Raymond-Smith code) with cosmic abundances and low energy absorption.

NGC 1553 We have obtained the spectral distribution of the counts in the whole $7'$ circle and in the inner $2'$ region. To these, a properly rescaled and vignetting-corrected background has been subtracted (see PROS documentation). A one temperature spectral fit to both regions does not give a satisfactory result: the best fit χ^2 value is high and the best fit low energy absorption

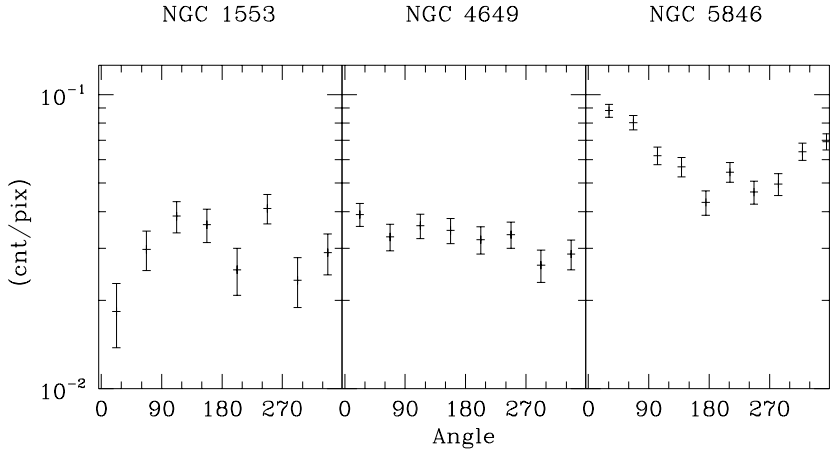

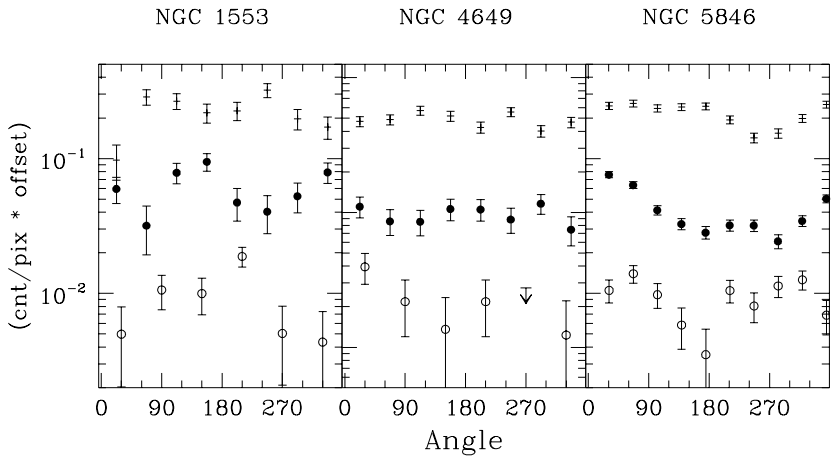

Fig. 7. Azimuthal distribution of the emission within a circle of $5'$ (NGC 1553 and NGC 4649) and $7'$ (NGC 5846) is shown in the upper panel. In the lower panels, the azimuthal distribution in different annuli is plotted. Crosses are for the $0' - 1'$ annulus, filled circles for the $1'$–$3'$ (NGC 1553 and NGC 4649) and $1' - 2.'5$ (NGC 5846) annuli; and open circles for the $3'$–$5'$ (NGC 1553 and NGC 4649) and $2.'5$–$5'$ (NGC 5846) annuli. A 3σ upper limit is calculated for the outermost annulus of NGC 4649 at angles 240°–300°.

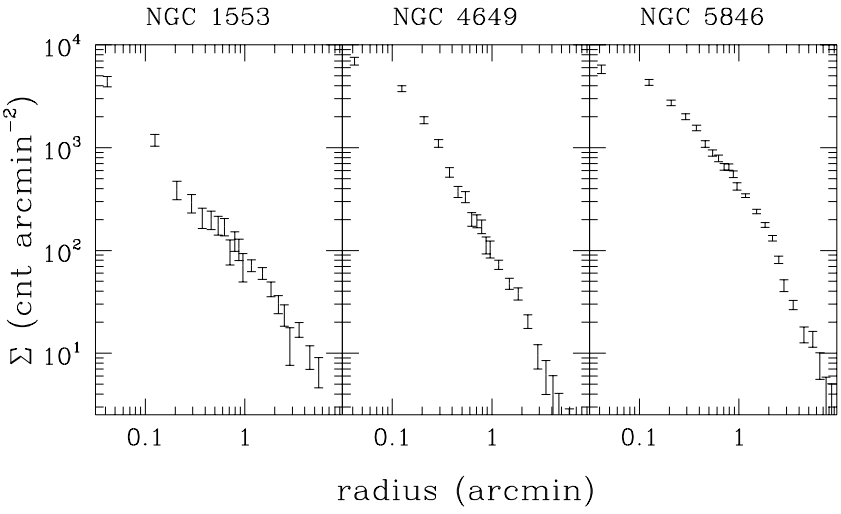

Fig. 8. Radial distribution of the net surface brightness emission from the sample galaxies

would imply a column density much lower than the line-of-sight value of 2.4×10^{20} cm^{-2}. Fixing the low energy absorption at the line-of-sight N_H column results in even poorer fits. The spectrum also seems much harder than usually found in bright early type galaxies (see Table 2).

We have therefore tried a two component fit, using two Raymond-Smith models with cosmic abundances. As shown by Table 2, this reduces significantly the best fit χ^2 value, and suggests that a very soft ~ 0.1 keV and a harder ~ 1 keV plasma could describe the data, if the absorbing column is fixed at the galactic value. The two components appear to contribute similar amounts in the inner $0'$–$2'$ circle, while the ~ 1 keV component contributes $\sim 60\%$ of the total extended emission.

Table 4. Fluxes and luminosities for the galaxies and their components

Galaxy	RA	Dec	Radius	net counts	error	flux ($\times 10^{13}$)	Luminosity	Notes
	J2000		$''$			erg cm^{-2} s^{-1}	erg s^{-1}	
NGC 1553	4 16 10.3	-55 46 48	300	2132.4	137.4	26.0	1.44×10^{41}	HRI; A
			420	1587.6	76.9	19.6	1.08×10^{41}	PSPC
central source	4 16 10.3	-55 46 48	15	203.4	17.0	2.48	1.37×10^{40}	B
N. feature 1	4 16 06.5	-55 45 24	20	38.0	11.0	0.46	0.26×10^{40}	C
N. feature 2	4 16 01.5	-55 45 54	20	36.6	11.0	0.45	0.25×10^{40}	C
West. P. S.	4 16 03	-55 46 54	15	29.6	9.6	0.36	0.20×10^{40}	D
central diffuse	4 16 11.5	-55 46 52	80×120	332.4	26.4	4.05	2.24×10^{40}	E
tail feature	4 16 17.5	-55 47 50	50×65	50.9	17.7	0.62	0.34×10^{40}	F
NGC 4649	12 43 40	11 33 10	420	2346.4	132.8	43.7	1.52×10^{41}	HRI
			420	5890	103	46.2	1.61×10^{41}	PSPC; G
NGC 5846	15 06 29.2	1 36 24	420	8508.9	250.6	69.2	1.74×10^{42}	HRI
			300	5982.7	96.6	50.6	1.27×10^{42}	PSPC
NNE feature			(60-150)	688	53	5.19	1.31×10^{41}	H

NOTES: No correction is applied to the flux estimate to account for photons scattered outside the source region. Fluxes are estimated using the best fit parameters obtained in Sect. 3 (see Tables 2 and 3). HRI/PSPC indicate the instrument used to derive the total flux. All other values are from the HRI data. Total fluxes are estimated within a radius of $\sim$ 30 (45), 35, and 90 (65) kpc for NGC 1553, NGC 4649 and NGC 5846 respectively.

A The source at 4:16:51 -55:49 has been masked out

B The background is taken in the adjacent annulus with $60''$ outer radius.

C The background is obtained in the annulus at the same radial distance from the peak (excluding the regions occupied by the two sources).

D The background is obtained from the Eastern half of the adjacent $20''$–$100''$ annulus

E The counts are obtained in a $80'' \times 120''$ box. The background is obtained in the adjacent rectangular annulus with outer dimensions of $160''$ and $240''$.

F The counts are obtained in a $50'' \times 65''$ box. The background is obtained in the Southern half of the annulus concentric to the box, and with $45''$–$80''$ inner and outer radii respectively, to avoid the central emission from the galaxy.

G From Trinchieri et al. (1997)

H Excess counts in the 340°–85° sector of the $1'$–$2.'5$ annulus, above the average emission in the 85°–340° at the same angular distance.

NGC 5846 The source region of NGC 5846 has been divided into 4 concentric annuli, and a spectral fit has been done on each. We have used two separate background estimates. For each annulus, we have used the $25'$–$27'$ region that should provide the shape and level of the background external to the galaxy; and we have used the adjacent outer annulus to each annulus analyzed (with the exception of the outermost one, as detailed in the notes of Table 3), in an attempt to subtract in part the contribution from the outer regions that are projected onto the innermost part (note that a proper procedure to disentangle the two contributions would require a more sophisticated spatial/spectral deconvolution of the data). The results are summarized in Table 3.

It is evident that the gas is cooler in the inner regions, as found in other early type galaxies (cf. Trinchieri et al. 1997), and that the temperature is an increasing function of radius. This evidence is stronger when the "local" background is subtracted from the data, even though the statistics are poorer.

However, while the average temperature in the annulus might be an increasing function of radius, the presence of substructure suggests that the average value might not apply everywhere in the annulus. For example, a significant feature is present in the $1' - 2.'5$ annulus, where enhanced emission is clearly observed in the HRI data to the NNE (Fig. 6). We have therefore checked whether the observed enhancement corresponds to different spectral characteristics of the emission.

We have divided the $1'$–$2.'5$ annulus in two separate regions, one between the angular limits 85°–340° and the other in the complementary region, and measured the spectral characteristics of the two regions separately. The background is estimated in the $2.'5 - 4'$ annulus. For the 340°–85° sector where the feature is we have also used as background the 85°–340° region at the same radial distance. The results are summarized in Table 3.

The region of the filament is cooler than the rest of the annulus, with kT$<$ 0.76–0.78 keV compared to kT$>$ 0.76 keV (90% values).

4. Fluxes, luminosities and densities of the hot gas

The spectral results above have been used to derive the global luminosity of these galaxies and to estimate the emission from the substructures in NGC 1553 and NGC 5846 (see Table 4). We have used the best fit spectral parameters to convert from HRI count rates to 0.1–2 keV fluxes. Luminosities are derived from the assumed distances of 21.5, 17 and 45.8 Mpc, for NGC 1553,

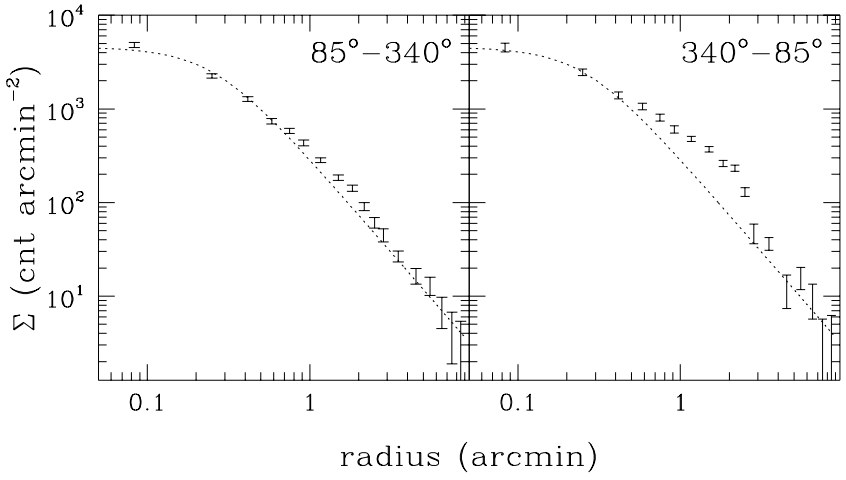

Fig. 9. Radial distribution of the net surface brightness emission of NGC 5846 in different angular sectors.

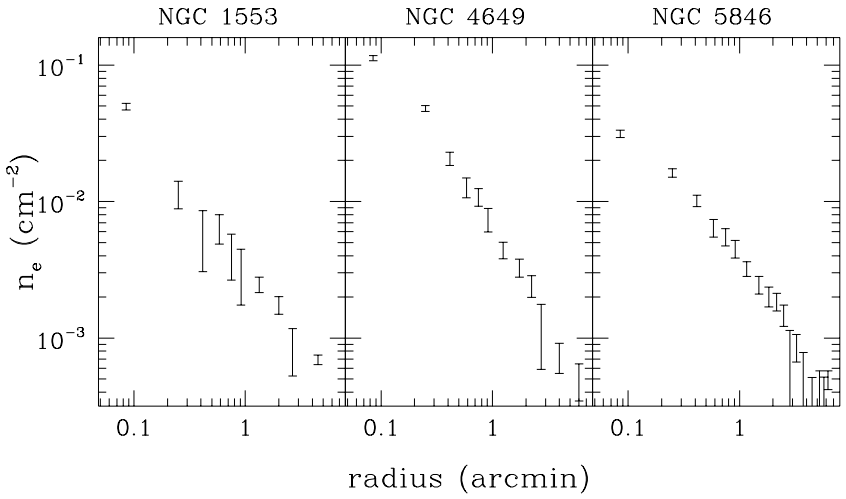

Fig. 10. Density profiles derived from the average surface brightness deprojected under the assumption of spherical symmetry. Central densities have been derived without taking into account the effects of the PSF.

NGC 4649 and NGC 5846 respectively. Total luminosities derived from the PSPC data are also listed for completeness.

The maps of both NGC 1553 and NGC 5846 show evidence of inhomogeneities on small and on larger scales. Table 4 lists the observed counts and luminosity of the two relatively isolated features observed in the NW quadrant in NGC 1553. At the present time it is not clear what the nature of these "clumps" is. Their luminosities, of a few $\times 10^{39}$ erg s^{-1}, is high compared to individual sources in our Galaxy, and in more normal spiral galaxies, and only comparable to the more extreme sources observed for example in the interacting pair "The Antennae" (Read et al. 1995) associated with very active HII regions (see also Williams & Chu 1995). If these small scale inhomogeneities are relatively widespread as suggested by the map of NGC 5846, it is likely that they are clumps in the gas distribution, rather than individual HII regions. Detailed deep optical observations would also help in determining the nature of these sources.

Gas densities can also be derived in different regions. However, as already extensively discussed elsewhere (see Trinchieri et al. 1997 and references therein), a number of assumptions have to be made about the state of the gas and the geometry, to obtain intrinsic values from the projected quantities that can be observed. Probably the more serious source of uncertainties is related to the volume assumed to derive gas densities, since the emission is clearly structured. In Fig. 10 we show the density profiles derived for the three galaxies from the average surface brightness profiles obtained in Sect. 2.3, deprojected under the assumption of spherical symmetry (Kriss et al. 1983), for the average temperatures derived in Sect. 3. For NGC 1553, for which a two temperature model is required, we have used kT= 1.008 keV (the value of the high temperature component). For NGC 5846 we have used the profile averaged over 360°. We have not taken into account the effect of the PSF in the innermost regions of the profile, therefore central densities are not accurate. Moreover, the innermost points in NGC 1553 are dominated by the point-like source, and should therefore be disregarded for the purpose of central density estimates. In fact, if we use the "King-type" model as input to the program to calculate the density profile, central densities are $n_e \sim 10^{-4}$ cm^{-3}. The total amount of hot gas in these galaxies is $M_{gas} \sim 0.4 - 4 \times 10^{10}$ $M_\odot$, and cooling times are shorter than $\sim 10^{10}$ yr out to the outermost radius used in these estimates, and are 10^7–10^8 yr in the innermost regions.

Given the clumpy nature of the emission however we expect that locally the gas could have significantly different densities than those derived on the average at different radii. We have es-

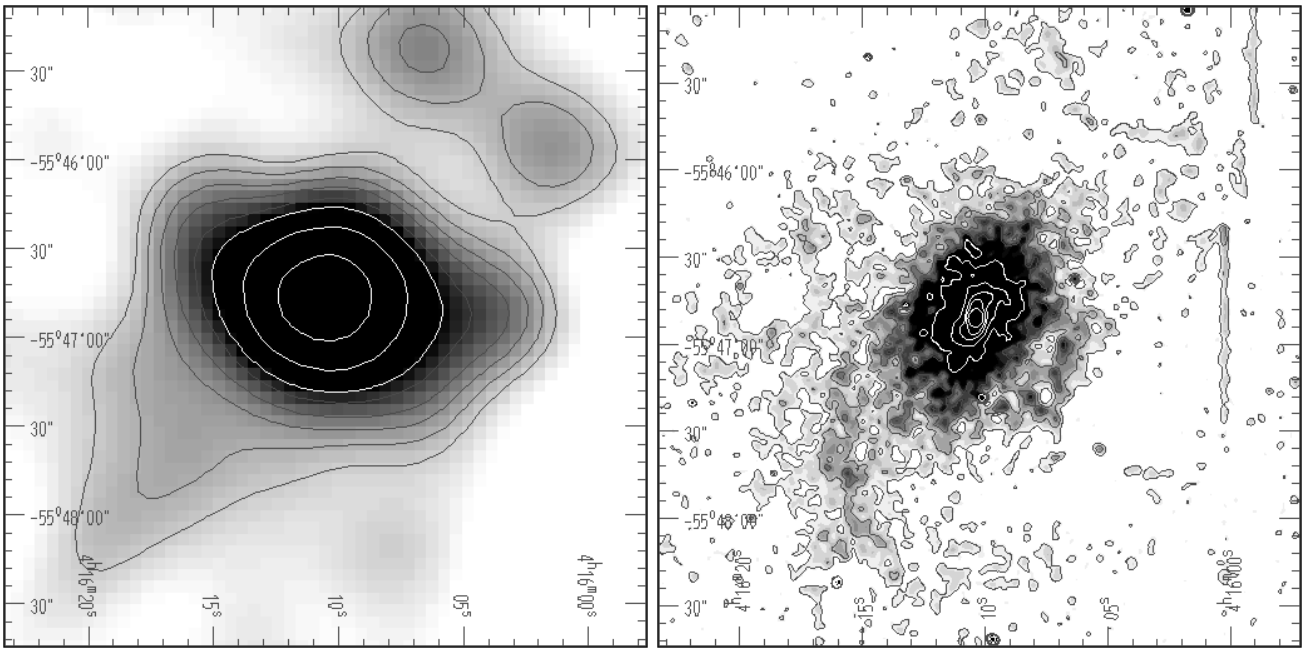

Fig. 11. Comparison between the Hα and X-ray morphologies for NGC 1553. The X-ray data (left) are on the same scale as the Hα data (right) from di Serego et al. (in preparation). The celestial coordinates of the Hα map have been assigned a posteriori without proper absolute calibration (the peak position was assigned the RC3 coordinates of the nucleus of NGC 1553). A Gaussian smoothing with σ= 2.5 pixel ($\sim 1''$) is applied to the raw data to enhance the low surface brightness features.

timated the density in three regions: the clumps to the NW and the tail to the SE observed in NGC 1553 and the NNE feature of NGC 5846 (see Table 2 and Table 3). Assuming spherical geometry and a radius of 2 kpc for the clumps ($20''$), we derive a density of $n_e \sim 0.02$ cm^{-3} in each clump. The estimate of the volume occupied by the other two features is not as straightforward. We have assumed a cylinder. For NGC 1553, the height h and the radius of the base b are h = 2.6 and b = 6.8 kpc ($25''$ and $65''$ respectively). The density in this region is therefore $n_e \sim 0.01$ cm^{-3}. For NGC 5846, assuming h = 20 kpc ($1.'5$) and b = 3.9 kpc ($0.'3$) for the cylinder, $n_e \sim 0.025$ cm^{-3}. Although these numbers should be taken with caution, since their estimate relies heavily on the volume assumed, they are indicative of large fluctuations in the local density, which could be $\sim$ 10 times higher than the average value derived at the same radial distance (see Fig. 10).

5. Comparison between X-ray and Hα emissions

The analysis of the Hα data for NGC 4649 and NGC 5846, obtained with the ESO 3.6 meter telescope at La Silla have been presented in Trinchieri & di Serego (1991). NGC 1553 will be presented in a forthcoming paper. Here we give a very brief description of the data quality and analysis performed to obtain the maps that we compare to the X-ray data. NGC 1553 was observed with the ESO EMMI at the NTT telescope in La Silla, Chile. The CCD detector used has a pixel size of $0.''4398$ and a total field of view of $7.'5 \times 7.'5$. To better remove spurious features, two exposures with a typical spatial offset of $\pm 10''$ in RA were obtained through a narrow band filter centered on the redshifted Hα line, and through the broad band r filter. To obtain sky subtracted, flat fielded images in each filter we followed a reduction procedure very similar to what we had used before (Trinchieri & di Serego 1991). The red image was then properly scaled and realigned to the Hα filter image and subtracted from it. Flux calibration was done using the standard stars observed in the same night with the same instrument.

Two of the galaxies analyzed here, NGC 1553 and NGC 5846, show a very complex Hα morphology. In both cases, the emission is not azimuthally symmetric, and filaments and substructures can be clearly identified. On the contrary, the Hα map of NGC 4649 shows little deviations from azimuthal symmetry and appears relatively smooth (Fig. 11, 12, 13). As already discussed in the previous sections, structures are also observed in the X-ray emission of NGC 1553 and NGC 5846, while the map of NGC 4649 shows a more regular, azimuthally symmetric morphology.

NGC 1553: The comparison between the X-ray and Hα maps is shown in Fig. 11. The Hα map enhances the low surface brightness features at larger radii, for a more significant comparison with the X-ray data. The line emission of NGC 1553 shows a strong nuclear peak and a bar-like feature in the $\sim$ NS direction that ends in a spiral structure at $\sim 8''$ from the nucleus. A more diffuse elliptical halo, with orientation and ellipticity similar to that of the stars, surrounds this inner structure and extends out to a a radial distance of $r \sim 40''$, outside of which fainter filaments and structures to the the SW and to the NW can be seen.

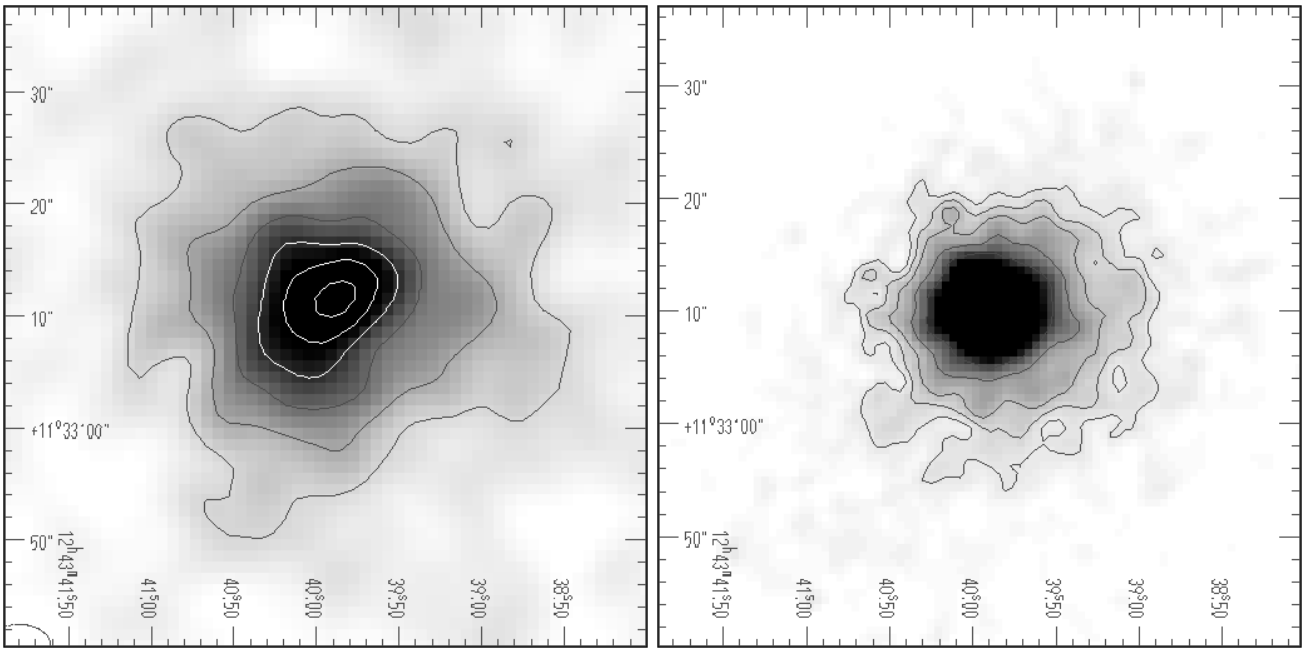

Fig. 12. Comparison between the Hα and X-ray morphologies for NGC 4649. he X-ray data (left) are on the same scale as the Hα data (right), from Trinchieri & di Serego (1991). A Gaussian smoothing with σ = 1.1 pixel ($\sim 0\farcs75$) is applied to the Hα data. The celestial coordinates of the Hα map have been assigned a posteriori without proper absolute calibration (by assigning the celestial coordinates to one star to the NE of the galaxy' nucleus obtained from the Guide Star Catalog; the star is not visible in this portion of the field).

The structure present in the central parts of the Hα, mostly confined to the inner $\sim 8''$, is not easily comparable with the X-ray data, both because of the poorer spatial resolution and limited statistics, and because of the presence of a central source in the X-ray data as well that would dwarf any lower level structure. At larger radii, outside of the more diffuse emission elliptical in shape and closely resembling the stellar light, a faint tail extends to the SE, where a similar feature is observed in the X-ray emission, as shown by Fig. 11. Two filaments to the NW, at a radial distance of $1.'5$ from the central peak, are spatially coincident with two features in the X-ray map.

NGC 4649: The comparison between the Hα and X-ray images indicates a lack of small scale features in both. The centrally peaked, roughly azimuthal symmetry out to $r \sim 30''$ in the Hα data is comparable to that observed in the X-ray map both in the same area covered by the line emission (Fig. 12) and out to a larger scale of $r \sim 5'$.

NGC 5846: A complex line emission peaked on the nucleus is visible in the inner $r \sim 30''$. The filamentary structure shows in particular a clear finger-like feature in the NE quadrant. (Fig. 13). Several of the Hα features seem to have a correspondence in the X-ray morphology, even though often this is more a qualitative than a quantitative statement. In particular, the Hα filament to the NE has a corresponding feature in the same quadrant and similar direction in the X-ray map. The scale of the X-ray feature is however not the same as the Hα: while this latter is visible at $30''$ to $60''$ from the central peak, the X-ray feature extends out to $\sim 2'$–$2.'5$. At smaller radii, there is not a coherent structure in the X-ray map, although excess emission starts at $\sim 30''$ in the NNE quadrant (see Fig. 9) and an indication of a beginning is visible in the X-ray contours.

6. Discussion

High resolution observations of three X-ray bright early type galaxies have shown a very complex morphology for two of these objects. Given the high X-ray luminosity, it is expected that the X-ray emission is dominated by the radiation of the hot interstellar medium, as shown by the statistical study of a sample of early type galaxies observed with the *Einstein* observatory (Trinchieri and Fabbiano 1985; Canizares et al. 1987; Kim et al. 1992). The mean spectral characteristics are also consistent with emission from hot gas. The characteristics of this gas indicate that it can cool on short timescales, and more so in the denser, cooler central regions. However, local variations in luminosity, temperature and density can exist on scales of arcseconds (or a few hundred pc at the distance of NGC 5846). Given the limited statistical significance of the emission in the outer regions of these objects, it is not possible with the present data to establish whether the emission is inhomogeneous only in the central regions, or it is clumpy everywhere. In the best studied example, NGC 5846, small scale inhomogeneities can be observed out to a distance of $r \sim 1'$ ($\sim$ 13 kpc). Features on larger scales and more coherent structures can however be followed to much larger distances: the extension in the NE quadrant is detected out to a radius $r \geq 3'$ ($\sim$ 40 kpc). It is at the

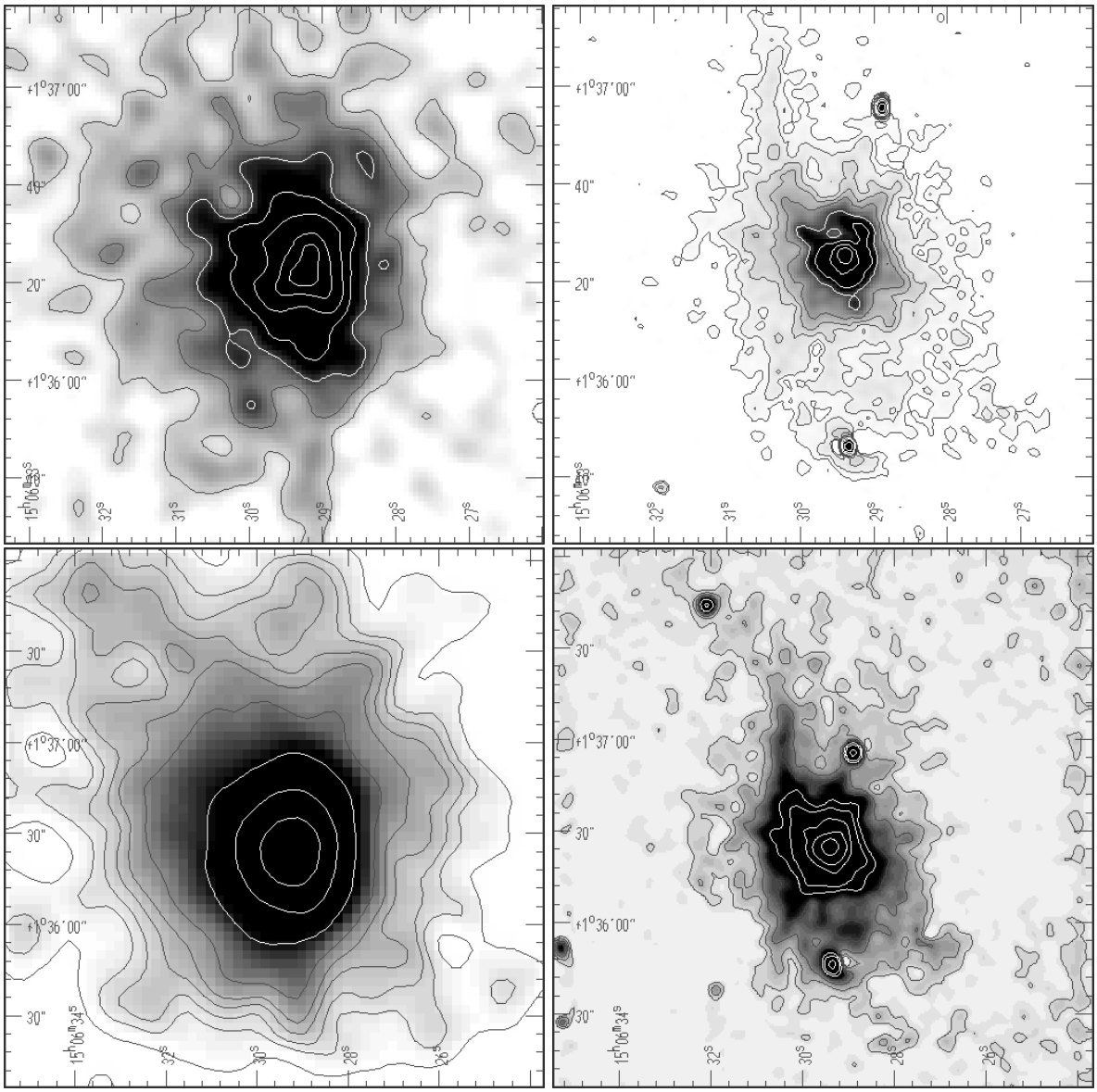

Fig. 13. Comparison between the Hα and X-ray morphologies for NGC 5846. The X-ray maps correspond to Fig. 6a–da (top left) and Fig. 6a–db (bottom left). The Hα data (right) are from Trinchieri & di Serego (1991), and have been smoothed with a Gaussian function of 1.2 and 2.5 pixels ($\sim 0\farcs8$ and $1\farcs7$, top and bottom panels respectively) to enhance features on different scales. The scale is the same in the two top and the two bottom figures, respectively. The celestial coordinates of the Hα maps have been assigned a posteriori without proper absolute calibration (the peak position is at the nucleus of NGC 5846 and has RC3 coordinates).

same time clear that inhomogeneities are not observed in all of the galaxies, in spite of the similar global X-ray properties, such as luminosity, gas temperatures and densities. The third object discussed here, NGC 4649, also the closest of the three, has a smoother and more regular emission at all scales. While it might be premature to draw general conclusions on the basis of 3 objects, it seems likely that the clumpyness of the emission is not intrinsic to the X-ray emission, but that it is linked to some other property of these galaxies. A larger data sample, observed at several frequencies, might provide us with some clues as to the nature of these "other" properties.

A second, very intriguing observational result is that of a spatial correlation between X-ray- and Hα-emitting features in the central regions of these galaxies, and in particular both the evidence of similar small and large scale features at both wavelengths **and** the lack of features at both wavelengths. Even though it is based on a sample of three objects only, this suggests a very close link between these two phases of the interstellar medium that needs to be understood.

Line emission observed in association with the presence of a cooling flow in clusters of galaxies has been originally interpreted as originating directly from the cooling of the 10^7 K

gas. By analogy, this mechanism would also work in early-type galaxies. However the expected intensity of the lines, for reasonable assumptions of the recombination rate, is significantly below the values observed (Johnstone et al. 1987, Trinchieri & di Serego 1991, and references therein). Several mechanisms have been investigated to explain the extended Hα emission in early type galaxies, and, in the absence of nuclear activity (as for example in Radio Galaxies, Heckman et al. 1989), photoionization from the available stellar population seems to be the most viable one (Trinchieri & di Serego 1991; Singh et al. 1994; and references therein). di Serego et al. (1990) and Trinchieri & di Serego (1991) proposed in particular that the old stars, like Post Asymptotic Giant Branch objects, might provide enough ionizing photons. Binette et al. (1994) have further shown that indeed old stars provide sufficient ionizing photons to explain the observed Hα luminosities. While properly accounting for the energetic requirement, such a mechanism would not explain however the peculiar morphology of some of these systems, since the ionizing photons are expected to be evenly distributed in the galaxy (in particular they would follow the stellar distribution), nor would it explain the close connection between very hot and warm gas.

Peculiar morphologies of the line emission could be explained by an uneven distribution of the cold gas, that would more strongly reflect the effects of an evenly distributed photoionizing field where it is denser. However, it is expected that the cold and hot gas have different origins (external for the cold component, and from stellar mass loss for the hot component), and therefore the distribution of the cold gas should have no effect on the morphology of the X-ray emission. One could however postulate that there exists a common mechanism that models the distribution of the gas at all observed phases. Magnetic fields and radio structures could provide such a mechanism. Displacement of thermal plasma has been detected in several clusters where maxima in the extended radio structures (radio lobes) correspond to minima in the X-ray emission (Sarazin et al. 1992, 1995, Böhringer et al. 1993, Carilli et al. 1993). However, neither NGC 1553 nor NGC 5846 are known to host structured strong radio sources (Slee et al. 1994, Fabbiano et al. 1989). In fact, only NGC 4649, that shows no peculiar morphology in either Hα or X-ray, shows a weak radio jet (Stanger & Warwick 1986). While the lack of radio emission does not guarantee the absence of magnetic forces and turbulences, it is likely that such mechanism is more relevant for galaxies hosting strong radio sources.

External mechanisms could also act on the gas in galaxies. Tidal forces could be invoked for example to explain the peculiar gas distribution of NGC 1553, probably interacting with NGC 1549 (Rampazzo 1988, Kormendy 1984). However, NGC 5846 is at the center of a small group and it is not known to be in interaction. Merging with a smaller group member cannot be dismissed, even though further analysis of the dynamical field should be done to clarify this possibility. However, if external mechanisms are acting on the gas, coherent features on relatively large scales should result. We could therefore interpret the inner large scale structures and the tail of NGC 1553 as resulting from the interaction with NGC 1549 (see also the simulations on the gas distributions of interacting galaxies by Noguchi 1990). However, small scale clumps are more difficult to interpret in this scenario. A more direct, and probably localized, link between hot and warm gas seems to be therefore required to explain the observed similarities.

Two models have been proposed that would provide a link between these two gas phases.

Voit & Donahue (1990) and Donahue & Voit (1991) present a theoretical model based on the assumption that the optically emitting filaments are powered by the radiation from gas emitting in the X-rays and EUV that predicts a high efficiency for converting soft X-ray photons into optical line emission, and therefore is able not only to reproduce the line ratios observed, but also to account for the high luminosity of the optical emission lines. Sparks et al. (1989) suggest that heat transfer from the X-ray gas to dust, which is often found to be associated with these optical line filaments might provide the excitation for the line emission. Their model, applied to the data of NGC 4696, explains their observations quite well.

As already discussed, we do not require a $source$ of ionizing photons in early type galaxies, since the stellar population can adequately supply the ionization needed. We do need however to explain the peculiar coincidences in the morphologies.

We need to consider a third component of the interstellar medium of these objects, which is found associated with the cold gas: dust. Dust has been observed in early type galaxies both through their far infrared emission and from direct observations of obscuring material in the optical. Since an external origin is expected for both cold gas and dust (Bertola et al. 1992 and references therein, Forbes 1991), it is likely that these two components have been acquired at the same time and that their distributions in the galaxies are similar (see also Kim 1989). Dust is known to be quite efficient in cooling the hot gas (see Cowie and Mckee 1977). We can therefore expect excesses in the X-ray emission coupled with the presence of dust, which favors heat conduction from the hot gas to the cooler material. As shown by the map of Trinchieri & di Serego (1991), there are two dust filaments in NGC 5846, one of which is in the general direction of the feature in the NE quadrant (see also Gallagher 1986; Ebneter et al. 1988). Dust is also observed in the central region of NGC 1553 (di Serego et al. in preparation; this galaxy is also detected in all four IRAS bands, Bally and Thronson 1989). It is therefore plausible that dust acts as a cooling agent throughout the region where the peculiar Hα and X-ray morphologies are observed. Clearly more detailed observations of all these components in a larger sample of galaxies are required to confirm their spatial correspondence and their close, causal connection. In particular, the importance of dust will be more extensively discussed in a forthcoming paper in light of more sensitive and more detailed observations of dust in NGC 5846 (Goudfrooij & Trinchieri, 1996 and in preparation).

7. Conclusions

The high resolution images of three high X-ray luminosity early type galaxies reveal the presence of inhomogeneities and structures in the morphology of the hot gas in both NGC 1553 and NGC 5846, while the central regions of NGC 4649 appear roughly azimuthally symmetric and smooth. These features appear at the centers both as (positive or negative) clumps in a more diffuse emission, on scales of a few arcsec, and as more coherent structures such as filaments/tails on scales of the order of arcminutes. PSPC spectral data of NGC 5846 indicate a significantly cooler temperature in one such feature, which suggests a ~ 10 times denser medium in the area.

An intriguing similarity is found between features in the Hα and X-ray maps of NGC 1553 and NGC 5846, while NGC 4649 shows no significant structures at either wavelengths. This suggests that a link exists between these two phases of the gas, that determines the spatial distribution of the emission. While it is unlikely that the morphologies of the hot and the cold gas could be both regulated by mechanisms like dynamical forces from a radio source in the galaxy or tidal forces with nearby companions, a possible link through heat conduction from hot gas to dust coupled to the cold, photoionized medium that gives rise to Hα features provides a reasonable explanation and accounts for the rough spatial coincidence of these three components of the interstellar medium.

Acknowledgements. GT thanks Dr. B. Aschenbach, S. Döbereiner, P. Goudfrooij and P. Rosati for useful and interesting discussions and for their comments on the manuscript. Dr. H. Böhringer and an anonymous referee have helped in improving the presentation of our work. This work was supported by the Agenzia Spaziale Italiana (ASI) and by NASA grant NAG5-2049 (ROSAT). GT acknowledges a Max-Planck Fellowship, where this work was finalized. This research has made use of the NASA/IPAC Extragalactic Database (NED) which is operated by the Jet Propulsion Laboratory, California Institute of Technology, under contract with the National Aeronautics and Space Administration.

References

Bally, J. and Thronson, H.A.Jr 1989 AJ 97, 69
Bertola, F., Buson, L.M., Zeilinger, W.W. 1992, ApJL 401, 79.
Binette, L. Magris, C.G., Stasońska, G. and Bruzual, A.G. 1994, AA 292, 13
Böhringer, H., Voges, W., Fabian, A.C., Edge, A.C. & Neumann, D.M. 1993 MNRAS 264, L25
Buson, L., Sadler, E.M, Zeilinger, W.W. et al. 1993, AA 280, 409
Carilli, C.L., Perley, R.A. & Harris, D.E. 1994, MNRAS 270 173
Canizares, C.R., Fabbiano, G. and Trinchieri, G. 1987, ApJ 312, 503
Cowie, L.L. and Mckee, C.F. 1977, ApJ 211 135.
David, L. et al. 1995 The ROSAT Users' Handbook
di Serego Alighieri, S., Trinchieri, G. and Brocato, E. 1990 in: Windows on Galaxies, G. Fabbiano, J.S. Gallagher and A. Renzini (eds.), Kluwer Academic Publishers, Dordrecht, p. 301.
Donahue, M. & Voit, G.M. 1991 ApJ 381, 361
Ebneter, K., Djorgovski, S., Davis, M. 1988, AJ 95 422
Fabbiano, G., Gioia, I.M. & Trinchieri, G. 1989 ApJ 347 127.
Forbes, D.A. 1991, MNRAS 249, 779
Gallagher, J.S. 1986, PASP 98 81
Goudfrooij, P., Hansel, L., Jorgensen, H-E. Norgaadrd-Nielsen, H.U. 1994, AAS 105, 341.
Goudfrooij, P. & Trinchieri, G. 1996 BAAS 28 1358
Heckman, T.M., Baum, S.A., vanBreugel, W.J.M., and McCarthy, P. 1989 ApJ 338 48.
Johnstone, R.M., Fabian, A.C., and Nulsen, P.E.J. 1987, MNRAS, 224, 75.
Kim, D.-W. 1989, ApJ 346, 653.
Kim, D.-W., Fabbiano, G and Trinchieri G. 1992, ApJ 393, 134
Kriss, G.A., Cioffi, D.F. & Canizares, C.R. 1983, ApJ 272, 439.
Kormendy J, 1984, ApJ 286, 116
Noguchi, M., 1990 "Dynamics and Interactions of Galaxies", R. Wielen (ed.), Springer-Verlag, p. 469
Rampazzo, R. 1988, AA 204, 81
Read A.M., Ponman T.J., Wolstencroft R.D., 1995, MNRAS 277, 397
Sarazin, C.L., O'Connel, R.W. & McNamara, B.R. 1992, ApJ 389, L59
Sarazin, C.L., Burns,J., Roettiger, K. & McNamara, B.R., 1995, ApJ 447, 559
Shields, JC. 1991, AJ 102, 1314
Singh K.P. Bhat P.N., Prabhu, T.P. and Kembhavi. A.K. 1995, AA 302, 658.
Slee O. et al. 1994, MNRAS 269, 928.
Sparks W.B., Macchetto, F. and Golombek, D. 1989, ApJ, 345, 153.
Stanger, V.J., & Warwick, R.S., 1986, MNRAS 220, 336.
Tody D., 1986, in Instrumentation in Astronomy VI, ed. D.L. Crawford (Proc. SPIE, vol. 627) 733.
Trinchieri, G. and Fabbiano, G. 1985 ApJ 296 447.296 447.
Trinchieri, G. & di Serego Alighieri S. 1991, AJ 101, 1647
Trinchieri, G., Fabbiano, G., Kim, D-W., 1997, AA, 318 361
Trinchieri, G., Kim, D-W., Fabbiano, G., & Canizares, C.R.C. 1994, ApJ 428, 555
Trinchieri G. & Noris L. 1995 in Röntgenstrahlung from the Universe, H-U. Zimmermann, J. Trümper, H. Yorke eds., 397
Voit, G.M. & Donahue, M. 1990 ApJ 360, L15
Williams, R.M. & Chu, Y.-H. 1995, ApJ 439, 132
Worrall, D.M. et al. 1992, in Data Analysis in Astronomy IV, ed. V. di Gesù et la. (New York: Plenum), 145.

This article was processed by the author using Springer-Verlag LaTeX A&A style file *L-AA* version 3.